HHS Public Access

Author manuscript

Nat Neurosci. Author manuscript; available in PMC 2019 July 21.

Published in final edited form as:

Nat Neurosci. 2019 March ; 22(3): 337–342. doi:10.1038/s41593-018-0321-z.

Acute silencing of hippocampal CA3 reveals a dominant role in place field responses

Heydar Davoudi[1,2,3,4] and **David J. Foster**[1,2,3,*]

[1]Department of Psychology, University of California, Berkeley, California 94720, USA

[2]Helen Wills Neuroscience Institute, University of California, Berkeley, California 94720, USA

[3]Solomon H. Snyder Department of Neuroscience, Johns Hopkins University School of Medicine, Baltimore, Maryland 21205, USA

[4]Department of Biomedical Engineering, Johns Hopkins University School of Medicine, Baltimore, Maryland 21205, USA

Abstract

Neurons in hippocampal output area CA1 are thought to exhibit redundancy across cortical and hippocampal inputs. Here we show instead that acute silencing of CA3 terminals drastically reduces place field responses for many CA1 neurons, while a smaller number are unaffected or have increased responses. These results imply that CA3 is the predominant driver of CA1 place cells under normal conditions, while also revealing heterogeneity in input dominance across cells.

The hippocampus plays a critical role in memory, and two systems-level mechanisms are thought to support this role: the spatially-localized responses of individual hippocampal neurons during locomotion, and the coordinated activity of large numbers of neurons during rest reflected in the local field potential (LFP) as high frequency (100-250Hz) sharp-wave-ripple (SWR) events[1]. The output area of the hippocampus, CA1, receives multiple excitatory inputs, including from entorhinal cortex and hippocampal CA3 and CA2, and numerous previous studies have suggested that redundancy governs their role in driving both place field responses[2–7] and ripple-related activity[5,7–9]. Early studies suppressing CA3 reported only minimal changes to CA1 place responses[2,3]. A recent molecular-genetic approach, blocking vesicle release at CA3 terminals, caused actually increased CA1 place field sizes, while peak firing rates were unaffected[4], as was ripple incidence in the LFP[5]. However, always the suppression of CA3 output was prolonged prior to the measurement of CA1 activity, either due to animal recovery and electrode adjustment following surgery[3], or the 6-8 weeks required for genetic expression[4,5]. Thus, compensatory changes such as

*corresponding author.

Contributions

H.D. and D.J.F. conceived the project, designed the experiments, and wrote the paper. H.D. performed the experiments and collected and analyzed the data.

Competing interest

The authors declare no competing interests.

homeostatic plasticity[10] might have occluded a more prominent role for CA3 input. We hypothesized that acute silencing of CA3 input would overcome this limitation.

We virally expressed either the light-activated proton pump eArch3.0 or GFP control in CA3 neurons in experimental (EXP, N=4) or control (CON, N=2) rats, respectively, using stereotaxic injections targeted specifically to CA3a,b at multiple sites along the septotemporal axis bilaterally (Fig. 1a and Supplementary Fig. 1a). After 4-6 weeks, expression of eArch3.0 in EXP rats was evident in CA3 cell bodies and in Schaffer collaterals in the stratum radiatum and stratum oriens of CA1, but not in the CA1 and CA2 stratum pyramidale (Fig. 1c-f **and** Supplementary Fig. 1b-c). In particular, while eArch3.0 was expressed in the axons of CA3 neurons passing through the CA2 subfield, co-labeling with CA2 cell bodies demonstrated almost no expression of eArch3.0 (Supplementary Fig. 1c). We used independently depth-adjustable optical fibers to illuminate CA3 terminals bilaterally in the stratum radiatum of dorsal CA1, while simultaneously recording from up to 40 independently depth-adjustable tetrodes gradually lowered bilaterally into the stratum pyramidale of dorsal CA1 (Fig. 1b and Supplementary Fig. 1d-e). To provide assurance that optical fibers were targeted to the stratum radiatum, a “piggyback” recording tetrode was attached to and flush with the bottom of each optical fiber. The incidence rate and amplitude of SWRs on the piggyback tetrodes matched the rest of the tetrodes, implying that they were at the same depth (Supplementary Fig. 2a-b). Hence, the light output was delivered to stratum radiatum and not to stratum oriens which was above and behind the fibers. We first examined the effect of acute CA3 suppression while rats were at rest in a sleep box (Supplementary Fig. 3a-b). In order to avoid over-estimation of effect size and significance by repetitive counting across successive recording sessions, only one session was selected for each tetrode per animal, from an initial baseline period before light delivery. This selection process yielded a total of 37 and 88 tetrodes in CON and EXP rats, respectively. The incidence of CA1 SWRs was dramatically suppressed in the majority of EXP tetrodes during light-on periods (ON) compared to light-off periods (OFF), while for CON tetrodes incidence was slightly enhanced (Fig. 1g-i and Supplementary Fig. 2c). There was some variability between EXP tetrodes likely due to variation between tetrodes in the amount of light impinging on axonal input, and indeed, the degree of SWR modulation for each tetrode correlated with estimated horizontal distance between tetrode and optical fiber tip for EXP tetrodes, but not for CON tetrodes (Fig. 1j). EXP tetrodes also exhibited a decrease in power spectral density in the ripple frequency band (Supplementary Fig. 2d). We also found subtle abnormalities in the expression of SWRs. Notably, the frequency of SWR peak power was decreased in EXP rats during ON periods, which is consistent with previous studies[5] (Supplementary Fig. 2e-g). There was a subtle rebound effect in light OFF periods revealed by comparing OFF periods with the initial baseline period. Although both EXP and CON tetrodes did not differ in SWR rate between OFF periods and the baseline, a second-order effect was observed in EXP animals only, in which the degree of negative modulation of SWR rate during ON compared to OFF was correlated with the degree of positive modulation of SWR rate during OFF compared to baseline (Supplementary Fig. 2h). Multi-unit spiking was also significantly suppressed in EXP tetrodes during the ON condition, while CON tetrodes were unaffected (Supplementary Fig. 2i-k). Similar results were found for awake SWRs, sampled from stopping periods punctuating periods of locomotive

behavior (Supplementary Fig. 4). Overall, these findings pinpoint CA3 as critical for the generation of SWRs and rest-state spiking activity in CA1.

We next considered the contribution of CA3 input to CA1 place field responses. Rats were trained in a linear track running task prior to recording, for 5–7 days, 30–40 laps (there and back) per day. We delivered light during alternate laps on the familiar linear track (Supplementary Fig. 3c). To avoid the possibility of repetitive inclusion of the same place cells from different sessions, we considered only one session for each tetrode based on the number of well-isolated clusters. 220 and 473 cell clusters were manually isolated from neural spike recordings from CON and EXP rats in different run sessions, respectively, of which 157 and 236 exhibited directional place fields (Fig. 2 and Supplementary Fig. 5). While illumination did not impair expression of place fields in CON place cells, around half of EXP place fields were substantially suppressed (EXP: 49.2%, CON: 3.8%; Fig. 2 and Supplementary Fig. 6). Moreover, 24.1% (28/116) of suppressed EXP fields were completely silenced, in that spiking was abolished. Interestingly, a very few cells enhanced their in-field activity (EXP: 8.1%, CON: 1.9%; Supplementary Fig. 6c) while the remaining cells were unaffected, in some instances possibly due to a lack of impinging light as noted above (EXP: 42.8%, CON: 94.3%). Overall, light caused a major reduction in firing rates in EXP fields, leading to lower in-field peak firing in field, smaller field size, increased spatial information per spike, and less stable yet sharper tuned fields (Fig. 2e-l, Supplementary Fig. 7). Importantly however, the increase in spatial precision did not reflect an increase in accuracy, rather the reverse was true: measures of the spatial location of the place fields, such as center of mass (COM) and spatial correlation, exhibited significant changes (Fig. 2g,k,l), although skewness was not significantly changed (Supplementary Fig. 7e-f), as changes to this measure are less detectable than for COM[11]. To examine whether CA3 merely augments spatial information available from other inputs such as cortex, or alternatively, transmits crucial spatial content unavailable from other inputs, we compared firing-matched place fields in light ON vs light OFF conditions, by downsampling spikes in whichever light condition had the higher total firing rate (Fig. 2i-l). While firing matching resulted in comparable place field peak firing modulation (Fig. 2i), it only partially captured the decrease in place field size (Fig. 2j) and lap-by-lap stability (Fig. 2m) and increase in spatial information (Supplementary Fig. 7b), in EXP rats. Moreover, the extent of the deviations in COM (Fig. 2k) and, critically, the decline in spatial correlation (Fig. 2l) in EXP rats were not captured at all by firing matching. These data establish that, for most neurons in the hippocampal output area, the spatial content of CA1 place fields depends heavily on CA3 input, even in a highly familiar environment, and cannot be supported solely by direct cortical input.

We noted that some tetrodes exhibited heterogeneity in the responses of their cells to CA3 suppression (Fig. 3a). Across all tetrodes, the proportion of each tetrode's cells that were excited, unaffected or suppressed varied, with many tetrodes exhibiting "mixed" populations of cells (Fig. 3b). We examined the locking of activity to hippocampal theta (Supplementary Fig. 8a-d). While the strength of phase locking remained unaffected by light in CON and EXP neurons, the mean phase of locking shifted to earlier phases. Phase precession was not affected by CA3 silencing, including the precession quality, slope, and range, consistent with a dependency on direct cortical input[12]. However, the onset phase was earlier, matching the

mean locking phase (Fig. 3c-e and Supplementary Fig. 8e-g and 9). Together, these results suggest that some cells are less dominated by CA3, and for these, CA3 contributes to the late phase of the theta cycle, consistent with a role in memory retrieval during theta sequences[13].

We speculated that a further contribution of CA3 might be revealed by examining the coordinated activity of CA1 ensembles. We performed Bayesian decoding of position during traversal of the linear track, revealing that position estimation was degraded in EXP rats in the light ON condition (Fig. 3f-g and Supplementary Fig. 10) The effect was not due to reduced spiking alone, consistent with the spatial correlation changes of individual cells' place fields (Fig. 3g). We further applied our analysis of coordinated activity to address replay during SWRs. Given our finding of a critical role of CA3 in SWRs, we hypothesized that replay would also be affected, and indeed replay quality was degraded in the light ON condition in EXP rats (Fig. 3h-i and Supplementary Fig. 11a). However, a complication for these analyses is the fact that many CA1 cells were not modulated by light condition, likely in part due to variability in light incidence. Therefore, we considered pairwise reactivation, separating pairs of cells both modulated by light during running ("suppressed" pairs) from pairs of cells both non-modulated ("intact" pairs). First, we examined whether the average time lag ("spike separation") between pairs during SWRs was modulated by light. While spike separation was not affected by light in intact pairs, it was decreased during light ON in suppressed pairs, and this effect was not due to lower spiking during light ON, as verified using the firing rate matching procedure (Fig. 3j-k). As a proxy for replay, it was expected that field pairs with spatially "close" field peaks would fire temporally close to each other during SWRs, while pairs with spatially "far" field peaks would fire with a higher spike separation[14,15]. We found that this pattern held for intact pairs regardless of light condition (Supplementary Fig. 11b), however it was only evident for suppressed pairs in the light OFF condition (Supplementary Fig. 11c). Further, when we applied the firing rate matching procedure to suppressed pairs, the pattern persisted in the light OFF condition, suggesting that spike rates alone could not account for the disruption to replay (Supplementary Fig. 11d). Taken together, these results define CA3 as critical not only for the generation of CA1 SWRs but also for their content.

Several possible caveats were mitigated as follows. Paradoxical increase in spontaneous vesicle release[16] was avoided by using short inactivation periods, and moreover we found only minor rebound effects of inhibition. A recent concern for off-target effects is less relevant here since rather than measuring a behavior dependent on the complex interaction of multiple circuits[17], we measured neural activity changes one synapse away. The proximity of area CA2 to the site of AAV injection was a potential concern, given its direct projection to CA1 and the temporal proximity of its activity to CA1 SWRs[8]. However, CA2 inputs synapse in the CA1 stratum oriens[18], which we avoided as indicated by both electrophysiological and anatomical evidence. The pattern of activity changes observed after suppression of CA3 input was hard to predict *a priori*, due to diversity in the polarity of projections from ipsilateral and contralateral CA3[19]. In summary, we found that a large fraction of individual CA1 neurons were critically dependent on CA3 input, even in a highly familiar environment, while a minority of cells may have been driven more by either cortical or CA2 inputs. Thus, while CA1 activity as a whole may depend on both CA3 and non-CA3 inputs[20], CA3 is the predominant driver of CA1 cells under normal conditions.

Online Methods

Animal training

A total of six adult male Long-Evans rats (2-3 months old, 250-400 g) were used for this study. All procedures were approved by Johns Hopkins University Animal Care and Use Committee and followed US National Institutes of Health animal use guidelines. Animals were housed on a standard, non-inverted, 12-h light cycle. Rats were food-restricted to achieve ~90% of their normal weight and then trained to traverse a 165-cm linear track to receive a liquid chocolate-flavored reward (200 μl, Carnation) at wells in either side of the track. Rats were trained for 30-40 complete laps once per day for 5-7 consecutive days on a familiar track. With this ~ 200 traversals, rats became highly familiar with the task, the track, and the environment.

Optogenetics setup

Each trained rat underwent two surgeries. The first surgery was for injecting adeno-associated virus (AAV) containing light-sensitive protein Archaerhodopsin (eArch3.0) to CA3. At least four weeks after injection, when CA3 cells bodies and axons strongly expressed eArch3.0 gene, the optetrode drive was implanted. The details of each of these steps are as follows.

Virus transduction (first surgery)—We chose AAV5 due to its transduction efficiency and high expression level of proton pump eArch3.0 in conjunction with a CamKIIa promotor that specifically targets pyramidal cells and not interneurons[21,22]. All viral constructs were provided from University of North Carolina Vector Core under material transfer agreement with Karl Deisseroth laboratory.

Four experimental (EXP) rats were injected with AAV5_CamKIIa_eArch3.0_EYFP and two control (CON) rats were injected with AAV5_CamKIIa_ EYFP in each of six sites in their dorsal and intermediate CA3a, and b. A total of 6 μL of virus (1 μL in each site) were stereotaxically injected in each rat (AP= −3.1 mm, ML = ±3.5, and DV= −3.5), (AP= −4.0 mm, ML = ±4.3, and DV= −4), and (AP= −4.7 mm, ML = ±4.8, and DV= −4.8) where AP, ML, and DV stand for anterior-posterior in relation to bregma, medio-lateral, and dorso-ventral axes in relation to surface of skull, respectively.

Optetrode design and implantation (second surgery)—A bilateral optetrode with two optical fibers (200 μm diameter) and up to 40 tetrodes (20 tetrodes in each hemisphere) was designed. For monitoring the position of each optical fiber in the brain, a “piggyback” tetrode was glued to and flush with the bottom of each optical fiber. Fibers and all tetrodes where independently adjustable. Each tetrode consists of a twisted bundle of four 17.8 μm platinum/10% iridium wires (Neuralynx, Boseman, MT), and by gold-plating the tip of each tetrode an impedance of <150 kΩ was achieved before implantation.

At least four weeks after viral injection, optetrodes were implanted on rats. Following surgical implantation, optical fibers and tetrodes were slowly lowered into the dorsal CA1 pyramidal layer over a few days using characteristic LFP patterns (mostly SWRs) and spiking patterns as a guide. Placement of tetrodes and recordings were performed as

previously described[23]. Optical fibers were adjusted to stay in stratum pyramidale, to be able to silence the stratum radiatum in dorsal CA1.

Immunohistochemistry and imaging

For localizing example tetrodes, five tetrodes in each hemisphere received electric lesion (20 μA DC current for 4 s) before perfusing a rat. Collected brains were fixed by 4% paraformaldehyde (PFA) in 0.1M sodium phosphate buffer (PBS), and preserved in 30% sucrose dissolved in PBS. 60 μm thick slices were prepared by cryostat and were mounted on slides. For defining CA2 region (PCP4 labeling), slices were first rinsed by 3×10 min PBS and for two hours were blocked by blocking buffer (3% normal donkey serum with 0.3% Triton-X in PBS). Then, slices were kept overnight in blocking buffer containing primary antibody (Rabbit α-PCP4, 1:500, Proteintech, Cat# 14705-1-AP). After 3×10 min PBS wash they were kept in blocking buffer containing secondary antibody (Alexa Fluor 594-conjugated donkey α-rabbit, 1:200, Invitrogen A21207). These antibodies have been validated in previous literature[24]. For background staining of the whole brain, after 3×10 min PBS wash, Hoechst 33258 (1:2,000) in PBS was applied to slices for 10 min and after 3×10 min PBS wash slices were covered with mounting media (Vectashield, Vector Laboratories Inc) and coverslip. Therefore, whole brain (blue signal via Hoechst 33258), CA3 cell bodies and axons (green signal via AAV-injected EYFP expression with no signal enhancement) and CA2 region (red signal, via PCP4 labeling) were imaged. Imaging was performed in Multiphoton Imaging (MPI) Core at Department of Neuroscience, Johns Hopkins University and CRL Molecular Imaging Center (MIC) at UC Berkeley. For tiled epifluorescence imaging of the whole brain and whole hippocampal area CA3 we used Zeiss Cell Observer and Zeiss AxioScan Z.1 systems. For high-resolution imaging of zoomed areas in CA3 and CA1 Zeiss LSM 510 confocal imaging system was used.

LFP and cellular unit recording

All data were collected using Digital Lynx data acquisition system (Neuralynx, Boseman, MT). The rat's position was tracked in darkness via blue and red LEDs mounted on the optetrode, and continuously recorded at 30 frames/s by an overhead camera. Analog neural signals were digitized at 32,000 Hz. The threshold for spike (extracellular action potential) detection was set to 50 μV. LFP data was digitally filtered between 0.1 and 500 Hz and recorded at 3,200 Hz after ten times downsampling. Individual units were also identified by manual clustering based on spike waveform peak amplitudes using a custom software (xclust2, Matthew A. Wilson, MIT).

Task design

A recording day consisted of a one-hour recording session in a sleep box ("Pre" rest session), followed by 20-35 traversing laps (lasting ~15-30 min) on a familiar 165 cm linear track ("Run" session), and one hour of recording in the sleep box ("Post" rest session). One limitation of optogenetic silencing using eArch3.0 is that minutes-long sustained illumination may paradoxically result in increased spontaneous vesicle release in axon terminals[16]. However, we avoided this issue by limiting our experimental design to shorter (< 1 min) inactivation of CA3 axons. In each rest session, light was delivered in four pulse trains, each lasting 400 seconds. Each pulse train consisted of alternating 20-s light on

stimulation periods followed by 20-s light off periods, with this on/off cycle repeating 10 times. Light was delivered from a 532 nm (green) laser and the estimated light power at the tips of optical fibers in each hemisphere was around 3.25 mW (light power density:100 mW/mm^2). Laser commands were generated by a custom-written MATLAB (Mathworks) graphic user interface and were delivered to laser by multifunction data acquisition device NI USB-6341(National Instruments).

Next, rats were put on a highly familiar linear track. For the Run session, light was manually and consecutively turned on and off for light ON and light OFF laps. For each light ON lap light was continuously on while the rat was traversing the track, staying at one end of the track and returning to the first position. For each rat, in different sessions, we usually switched the light stimulation paradigm on track to remove the bias of animal to one end of the track in the recording room. The stimulation paradigm for “Post” rest sessions where similar to “Pre” rest sessions.

Analysis

LFP analysis—All tetrodes that were able to detect SWRs (with incidence rate of more than 0.05 SWR/s in either light OFF or light ON conditions) were included in the LFP analysis, regardless of whether they showed any modulation by light or not. For SWR detection in the sleep box, only “pre” rest sessions where analyzed and, using a speed threshold of 7 cm/s, moments that rat intensely moved were excluded from the analysis. One electrode from each acceptable tetrode was considered for LFP analysis. To avoid repetitive measurements, for each tetrode only the session in which it had maximum baseline (5-10 min pre-stimulus recording) SWR incidence rate was selected. The LFP signal of each electrode was denoised for 60 Hz electric noise and its 180 Hz harmonic using a second-order IIR notch filter. Then, denoised LFP was filtered at SWR frequency range (100-250 Hz) with a fifth-order Butterworth band-pass filter. The envelopes of each band-passed LFP were obtained using the absolute value of its Hilbert transform. After applying a Gaussian smoothing filter with 5 ms standard deviation, the envelope was z-scored. Events that passed 5 standard deviations (i.e., mean + 5 SD of averaged non-z-scored envelope) were considered as candidate SWR events, and SWRs that were less than 10 ms apart were merged and considered as one extended ripple. The beginning and end of each SWR were defined as where the smoothed envelope crossed its one standard deviation value and events lasting less than 20 ms were removed. Tetrodes with SWR incidence rate of more than 0.05 SWR/s (e.g. at least one ripple event on average in every 20 s either during light OFF or light ON periods) were considered for further analysis.

Place field calculation and features—Due to manual commanding of laser, there was a variability in the start time of light ON laps. Therefore, the reward zones on either side of the track (17.5 cm each side) were excluded and only the middle130 cm of the 165-cm-long track was considered for place field calculation. All the place cell analyses, except spatial coherence, were done on 1-D place fields. 1-D place fields were obtained by binning the linear track using 2 cm bins, and the raw place field was smoothed by applying a Gaussian filter with a 5 cm SD. Also, all analyses were done independently on directional fields in light OFF and light ON conditions. To avoid repetitive inclusion of place cells from different

sessions, for each tetrode only the session in which it had most place cells was considered for analysis. To have a relatively inclusive definition, only cells that met all the following criteria either in light OFF or light ON conditions were considered as place cells. These consist of a peak field firing rate > 1 Hz, spatial coherence > 0.1, lap-by-lap stability > 0.2, and number of spiking laps >5. Moreover, place fields that covered the whole track with a low spatial information (< 0.15) were considered as truncated place fields and were omitted. Place field features were calculated as follows. Place field size was calculated as the number of contiguous 2-cm-wide bins above 20% of peak place field firing. For features such as peak firing rate and field size all place fields from light OFF and light ON conditions were included in the analysis (as far as field passed the aforementioned criteria at least in one light condition). For example, if a place field gets completely suppressed in light ON condition, its peak firing rate and field size become zero and included in the analysis. However, for the following features, only fields that passed the criteria in at least one light condition and had at least one spike in the other condition were included in the analysis.

The sparsity index ranges from 0 to 1, where a lower value means a less diffuse and more spatially-specific place field[25]. Sparsity is defined as:

$$\text{Sparsity} = \frac{(\sum_{i=1}^{n} p_i \cdot f_i)^2}{\sum_{i=1}^{n} p_i \cdot f_i^2}$$

Where each 2 cm bin (n = 65) has firing rate f_i and occupancy time t_i, and pi is the occupancy probability: $p_i = t_i / \sum_{i=1}^{n} t_i$.

Spatial information, which is the amount of information about an animal's position conveyed by each spike, is calculated as follows[25]:

$$\text{Spatial Information} = \sum_{i=1}^{n} p_i \frac{f_i}{f} log_2 \frac{f_i}{f}$$

Where f is the mean firing rate, $f = \sum_{i=1}^{n} p_i f_i$.

The center of mass (COM) of a place field was calculated using the following equation:

$$\text{COM} = \frac{\sum_{i=1}^{n} x_i \cdot f_i}{\sum_{i=1}^{n} f_i}$$

where x_i is the i-th position bin on the track.

The skewness of each place field was defined as:

$$\text{Skewness} = \frac{\sum_{i=1}^{n} f_i .(x_i - mean(x))^3}{\sigma_x^{3/2} \cdot \sum_{i=1}^{n} f_i}$$

with σ_x defined as:

$$\sigma_x = \frac{\sum_{i=1}^{n} f_i .(x_i - mean(x))^2}{\sum_{i=1}^{n} f_i}$$

Spatial coherence, which quantifies smoothness and local orderliness of a place field, is the autocorrelation of each place field with its nearest neighbor average[26]. To do this, the 6 × 130 cm linear track was binned into 2 × 2 cm bins and the new firing map for each pixel was calculated as the average firing rate of the eight unsmoothed neighbor pixels. Then, the 2-D correlation coefficient between the original unsmoothed firing map and the new one was calculated and to be statistically comparable we applied a Fisher transform (or z-transform, z = arctanh(r)) on correlation coefficients before calculating Z-values.

Lap-by-lap stability was defined as the average of the correlation of the place field each spiking lap with the overall place field. This measure was separately calculated for light OFF and light ON laps.

Spatial correlation, which was defined as the normalized Pearson correlation coefficient of place fields in light OFF and light ON conditions, was also Fisher-transformed for statistical comparison.

The modulation effect significance was calculated for each place field by comparing its lap-by-lap spike counts per second in light OFF vs. light ON laps. For each tetrode a 2-d heterogeneity value was defined as the percentage of its fields that were statistically significantly suppressed vs the percentage of its fields that were statistically significantly enhanced.

Place cell firing-matching—To test whether the partial suppression of CA3 input simply downsamples the number of CA1 place cell spikes or CA1 spatial coding is more systematically disrupted, the total firing rate of each place field was matched in light OFF and light ON conditions. For each correspond OFF and ON fields, the spikes of whichever field with higher total firing rate were randomly omitted to the extent of reaching a matched total firing rate. Then, all place field features were calculated for the firing-matched OFF and ON fields, separately for CON and EXP rats.

Theta phase locking and phase precession—For the temporal coding analysis, only place fields that not only passed the aforementioned criteria but also contained at least 10 in-field spikes in both light OFF and light ON conditions were considered for further theta phase locking and phase precession analysis. We chose these relatively low criteria to be more inclusive in studying the effect of field suppression on its temporal coding properties.

For each tetrode, instantaneous theta phase was calculated using Hilbert transform of theta-band filtered LFP. For each session, we chose a tetrode with high theta power as global reference theta. Then, for each place cell, spikes and LFP timestamps were used to linearly interpolate theta phase for each spike. The degree of modulation of each place cell by theta phase was obtained by calculating its circular mean resultant vector (MRV). MRV may vary from 0 (no phase preference) to 1 (every spike occurred at the same theta phase). To make recording sessions comparable, by using multi-unit activity of all the clustered cells, global reference theta was shifted in a way that maximum multi-unit firing occurs at the trough (180°) of theta rhythm. To calculate theta phase precession[25], circular-linear regression was used[27]. A linear model $\varphi(x) = 2\pi ax + \varphi_0$ was fit into phase-position circular-linear pairs $\{x_i, \varphi_i\}_{i=1}^{n}$ for each place cell independently for ON and OFF place fields. Precession slope a was varied between range $\mathbb{C} = (-10, 10)$, which is equivalent to (−27.69 °/cm, 27.69 °/cm), to find optimal $\hat{a} = argmax_{a\epsilon\mathbb{C}} R(a)$ that maximizes R(a), the MRV of the circular errors between the measured phase φ_i and the model predictions $\varphi(x)$:

$$R(a) = \sqrt{\left(\frac{1}{n}\sum_{i=1}^{n}\cos(\varphi_i - 2\pi a x_j)\right)^2 + \left(\frac{1}{n}\sum_{i=1}^{n}\sin(\varphi_i - 2\pi a x_j)\right)^2}$$

Next, phase offset $\hat{\varphi}_0$ is calculated as follows:

$$\hat{\varphi}_0 = arctan2\frac{\sum_{i=1}^{n}\sin(\varphi_i - 2\pi\hat{a}x_i)}{\sum_{i=1}^{n}\cos(\varphi_i - 2\pi\hat{a}x_i)}$$

Then, the circular-linear correlation coefficient is calculated as follows:

$$\rho = \frac{\sum_{i=1}^{n}\sin\left(\varphi_i - \overline{\varphi}\right)\sin\left(\theta_i - \overline{\theta}\right)}{\sqrt{\sum_{i=1}^{n}\sin\left(\varphi_i - \overline{\varphi}\right)^2 \sum_{i=1}^{n}\sin\left(\theta_i - \overline{\theta}\right)^2}}$$

where $\overline{\varphi} = \frac{\sum_{i=1}^{n}\sin\left(\varphi_i\right)}{\sum_{i=1}^{n}\cos\left(\varphi_i\right)}$ and $\overline{\theta} = \frac{\sum_{i=1}^{n}\sin\left(\theta_i\right)}{\sum_{i=1}^{n}\cos\left(\theta_i\right)}$, and $\theta_i = 2\pi|\hat{a}|x_i (mod\ 2\pi)$ is the linearly fitted phase. To determine statistical significance, the scaled correlation was calculated. For large n and under the null hypothesis that phases are from an uncorrelated Gaussian random distribution, the scaled correlation is given by

$$z = \rho\sqrt{n\frac{\lambda_{02}\lambda_{20}}{\lambda_{22}}}$$

where

$$\lambda_{ij} = \frac{1}{n}\sum_{k=1}^{n} \sin^{i}\left(\varphi_i - \overline{\varphi}\right)\sin^{j}\left(\theta_i - \overline{\theta}\right)$$

Given z, the significance value can be derived from the cumulative normal distribution:

$$p = 1 - \mathrm{erf}\left(\frac{|z|}{\sqrt{2}}\right).$$

Once the linear regression parameters were calculated, precession phase onset and range were respectively derived by the multiplication of the beginning and the size of a place field by the precession slope.

Neural population analysis

Bayesian decoding of position—A Bayesian probability-based decoding algorithm for estimating animal's position was performed[28]. The posterior probability (*Prob*) of the animal's position (*P*) in each running direction (*dir*) across N_P total position bins given a time window containing neural spiking (*spikes*) from N_F directional place fields is

$$Prob_{dir}(P|spikes) = U_{dir} / \sum_{j=1}^{N_P} U_{dir}$$

Where

$$U_{dir} = \prod_{i=1}^{N_F} f_i(P, dir)^{n_i} \exp(-i \sum_{i=1}^{N_F} f_i(P, dir))$$

and $f_I(P, dir)$ is the i-th place field in a running direction, assuming independent rates and Poisson firing statistics for all N fields and a uniform prior over position. n_i is the number of spikes in i-th place field in a time window of 400 ms which was used to estimate the rat's position on a behavioral timescale. This time window was slid by 50 ms timesteps. OFF fields were used for decoding position during both light OFF and light ON conditions because ON fields were highly suppressed resulting to an even more degraded decoding. Also, since rats did head sweeping beyond the ends of track we considered a 180 cm position range (15 cm extension to 165 cm track) for better decoding of behavior at the ends of track. For this purpose, we recalculated place fields and included cells that fired at the ends of track. This was only for visualization purpose and for run decoding error analysis we stayed with original 130-cm-range place fields.

Position reconstruction error during run was defined as the average distance between the animal's current location and the peak decoded position in each 200-ms time bin while rat was traversing the track with a > 7 cm/s speed. Chance level of reconstruction error was determined by performing the same calculation except substituting the peak decoded positions with random positions. To test whether the degradation in positional decoding is

merely due to lower spiking of place cells under light, we performed firing matching of individual place cells as described in “Place cell firing-matching” section and then recalculated the position reconstruction error.

Replay decoding and characterization—Each global SWR event (detected from average z-scored LFP of all tetrodes) was considered as a candidate population event in which a time window of 20 ms sliding in 5 ms steps was used to estimate position. Because replays start at the ends of track where rats are at rest or head sweeping we considered a 180 cm position range for Bayesian decoding of replays. To calculate the statistical significance of each candidate event with 2-d weighted correlation more than 0.5, place field identities were randomly shuffled for 1,000 times and p-value was calculated by Monte Carlo method: $p = (n + 1)/(s + 1)$, where s is the total number of shuffled data sets and n is the number of shuffled data sets that produced a number of correlated events greater than or equal to the correlation of candidate event. Candidate events with $p < 0.05$ were considered as replays. Replays were characterized with two measures, i.e. replay score, and replay speed. They were defined as where the likelihood (R) that a replay is along the fitted line with slope v and starting location ρ is maximized[28]. R was calculated as the averaged decoded probability in a vicinity (vic) along the fitted line:

$$R(v,\rho) = \frac{1}{N_T} \sum_{i=0}^{N_T - 1} \sum_{j \in vic} Prob_{ij}(|P - (\rho + v \,.\, i \,.\, \Delta t)| \leq d)$$

where Δt is the moving step of the decoding time window (5 ms) and the value of d was empirically set to 15 cm for capturing local variations in slope. If for a time bin i the fitted line would specify a location beyond the ends of the track, the median probability of all possible locations was taken as the likelihood. To determine the most likely slope for each replay, we densely sampled the parameter space of v and ρ to find the values $v_{\max}$ and $\rho_{\max}$ that together maximize R. Replay speed is defined as $|v_{\max}|$ in m/s and replay slope is the value of $R_{\max}$.

Pairwise reactivation analysis—To measure the degree to which cells fire with a certain time lag during SWRs, we took spike counts in consecutive 5-ms time bins during and in the vicinity (50 ms in each side) of SWRs, separately for light OFF and light ON conditions. Average time lag or “spike separation” of each pair was defined as the center of mass of absolute value of cross-correlation coefficient of two spike counts trains (50 bins = 250 ms sweeping in each temporal direction). Therefore, for each cell pair spike the separation measure was calculated separately for light OFF and light ON conditions. Correspondingly, spike separation modulation was defined as (ON−OFF)/(ON+OFF). To refine the effect of light on cell pairs we separated “suppressed” pairs, i.e. cell pairs that their associated place fields were both suppressed by light from “intact” pairs, i.e. cell pairs that their fields were unaffected by light. Cell pairs with complete suppression of either of their associated place fields during light OFF condition were excluded from the analysis. Moreover, a pair that either of its two spike count trains had less than 20 bins with non-zero value during light OFF condition were excluded from analysis. To investigate whether the

observed effects were due to less spiking during light ON condition we did a firing matching for in-SWR spike count trains. Spike downsampling for each spike count train was only applied whichever light condition had the higher in-SWR firing rate. The amount of downsampling was proportional to the ratio of in-SWR firing rate in the two light conditions. After averaging the 20-times random firing-matching of spike count trains, the spike separation for all “suppressed” pairs were calculated. Existence of replays predicts that field pairs with “close” field peaks will fire with a lower spike separation than pairs with “far” peaks. A threshold distance of 65 cm (i.e. half of the 130-cm running part of the track) was selected to define close vs far pairs. Distance between OFF fields were used for applying this threshold for both light OFF and light ON conditions. Consequently, spike separations were separately calculated for intact, suppressed, and firing-matched pairs during light OFF and light ON conditions.

Statistical analysis and reproducibility—No statistical methods were used to pre-determine sample sizes but our sample sizes are similar to those reported in previous publications[29]. Animals were randomly selected to be in either the CON or EXP groups by being injected either with GFP or eArch3.0, respectively. Data collection and analysis were not performed blind to the conditions of the experiments.

For most analyses, if data points had a Gaussian distribution (checked by Lilliefors test), depending on the type of comparison a two-tailed paired-sample or two-sample t-test was applied. For non-Gaussian distributions, depending on the type of comparison the non-parametric two-tailed paired-sample Wilcoxon signed rank test or two-tailed two-sample Wilcoxon rank sum test (aka Mann–Whitney U test) was used. The modulation index for each place field feature was defined as (ON − OFF)/(ON + OFF). For example, for place field peak modulation, a modulation index of −1 means complete suppression, 0 means no modulation, and a positive value means an enhancement in peak firing. For COM, this index was simply defined as (ON − OFF)/130. For circular statistics CircStat Matlab toolbox was used[30]. Circular Rayleigh test and Watson-Williams test were used respectively for test for non-uniformity and for comparison of two population phases.

Life Sciences Reporting Summary

Further information on research design is available in the Nature Research’s Life Sciences Reporting Summary linked to this article.

Data availability

The data that support the findings of this study are available from the corresponding author upon reasonable request.

Code availability

The code that support the findings of this study are available from the corresponding author upon reasonable request.

Supplementary Material

Refer to Web version on PubMed Central for supplementary material.

Acknowledgements

This work was supported by The McKnight Endowment Fund for Neuroscience (D.J.F.) and National Institute of Mental Health grant R01 MH103325 (D.J.F.). We thank Zeinab Vessal for graphic design. For imaging facility, we thank Michele Pucak at Multiphoton Imaging Core (center grant: P30 NINDS 050274) at Department of Neuroscience, Johns Hopkins University and Holly Aaron and Feather Ives at CRL Molecular Imaging Center (Biological Research Faculty Grant) at UC Berkeley.

References

1. Buzsáki G Hippocampal sharp wave-ripple: A cognitive biomarker for episodic memory and planning. Hippocampus 25, 1073–1188 (2015). [PubMed: 26135716]
2. Mizumori SJY, Mcnaughton BL, Barnes CA & Fox KB Preserved Spatial Coding in Hippocampal CA1 Pyramidal Cells During Reversible Suppression of CA3c Output: Evidence for Pattern Completion in Hippocampus. J. Neurosci 9, 3915–3928 (1989). [PubMed: 2585060]
3. Brun VH et al. Place Cells and Place Recognition Maintained by Direct Entorhinal-Hippocampal Circuitry. Science (80-.). 296, 2243–2246 (2002).
4. Nakashiba T, Young JZ, McHugh TJ, Derek L. Buhl & Tonegawa S Transgenic Inhibition of Synaptic Transmission Reveals Role of CA3 Output in Hippocampal Learning. Science (80-.). 1260, 1260–4 (2008).
5. Nakashiba T, Buhl DL, McHugh TJ & Tonegawa S Hippocampal CA3 Output Is Crucial for Ripple-Associated Reactivation and Consolidation of Memory. Neuron 62, 781–787 (2009). [PubMed: 19555647]
6. Brun VH et al. Impaired Spatial Representation in CA1 after Lesion of Direct Input from Entorhinal Cortex. Neuron 57, 290–302 (2008). [PubMed: 18215625]
7. Middleton SJ & McHugh TJ Silencing CA3 disrupts temporal coding in the CA1 ensemble. Nat. Neurosci 19, 945–51 (2016). [PubMed: 27239937]
8. Oliva A, Fernández-Ruiz A, Buzsáki G & Berényi A Role of Hippocampal CA2 Region in Triggering Sharp-Wave Ripples. Neuron 91, 1–14 (2016). [PubMed: 27387643]
9. Yamamoto J & Tonegawa S Direct Medial Entorhinal Cortex Input to Hippocampal CA1 Is Crucial for Extended Quiet Article Direct Medial Entorhinal Cortex Input to Hippocampal CA1 Is Crucial for Extended Quiet Awake Replay. Neuron 96, 217–227.e4 (2017). [PubMed: 28957670]
10. Keck T et al. Integrating Hebbian and homeostatic plasticity: the current state of the field and future research directions. Philos. Trans. R. Soc. London B Biol. Sci 372, (2017).
11. Roth ED, Yu X, Rao G & Knierim JJ Functional differences in the backward shifts of ca1 and ca3 place fields in novel and familiar environments. PLoS One (2012). doi:10.1371/journal.pone.0036035
12. Schlesiger MI et al. The medial entorhinal cortex is necessary for temporal organization of hippocampal neuronal activity. Nat. Neurosci 18, 1123–1132 (2015). [PubMed: 26120964]
13. Feng T, Silva D & Foster DJ Dissociation between the Experience-Dependent Development of Hippocampal Theta Sequences and Single-Trial Phase Precession. J. Neurosci 35, 4890–4902 (2015). [PubMed: 25810520]
14. Suh J, Foster DJ, Davoudi H, Wilson MA & Tonegawa S Impaired Hippocampal Ripple-Associated Replay in a Mouse Model of Schizophrenia. Neuron 80, (2013).
15. Karlsson MP & Frank LM Awake replay of remote experiences in the hippocampus. Nat. Neurosci 12, 913–918 (2009). [PubMed: 19525943]
16. Mahn M, Prigge M, Ron S, Levy R & Yizhar O Biophysical constraints of optogenetic inhibition at presynaptic terminals. Nat. Neurosci (2016). doi:10.1038/nn.4266
17. Otchy TM et al. Acute off-target effects of neural circuit manipulations. Nature 528, 358–363 (2015). [PubMed: 26649821]

18. Dudek SM, Alexander GM & Farris S Rediscovering area CA2: unique properties and functions. Nat. Rev. Neurosci 17, 89–102 (2016). [PubMed: 26806628]
19. Zugaro MB, Monconduit L & Buzsáki G Spike phase precession persists after transient intrahippocampal perturbation. Nat. Neurosci 8, 67–71 (2005). [PubMed: 15592464]
20. Ahmed OJ & Mehta MR The hippocampal rate code: anatomy, physiology and theory. Trends in Neurosciences 32, 329–338 (2009). [PubMed: 19406485]
21. Yizhar O, Fenno LE, Davidson TJ, Mogri M & Deisseroth K Optogenetics in Neural Systems. Neuron (2011). doi:10.1016/j.neuron.2011.06.004
22. Gradinaru V et al. Molecular and Cellular Approaches for Diversifying and Extending Optogenetics. Cell 141, 154–165 (2010). [PubMed: 20303157]
23. Foster DJ & Wilson MA Reverse replay of behavioural sequences in hippocampal place cells during the awake state. Nature 440, 680–3 (2006). [PubMed: 16474382]
24. Boehringer R et al. Chronic Loss of CA2 Transmission Leads to Hippocampal Hyperexcitability. Neuron (2017). doi:10.1016/j.neuron.2017.04.014
25. Skaggs WE, McNaughton BL, Wilson MA & Barnes CA Theta phase precession in hippocampal neuronal populations and the compression of temporal sequences. Hippocampus 6, 149–172 (1996). [PubMed: 8797016]
26. Muller RU, Kubie JL & Muller RU The firing of hippocampal place cells predicts the future position of freely moving rats. J. Neurosci 9, 4101–10 (1989). [PubMed: 2592993]
27. Kempter R, Leibold C, Buzs??ki G, Diba K & Schmidt R Quantifying circular-linear associations: Hippocampal phase precession. J. Neurosci. Methods 207, 113–124 (2012). [PubMed: 22487609]
28. Davidson TJ, Kloosterman F & Wilson MA Hippocampal Replay of Extended Experience. Neuron 63, 497–507 (2009). [PubMed: 19709631]
29. Rueckemann JW et al. Transient optogenetic inactivation of the medial entorhinal cortex biases the active population of hippocampal neurons. Hippocampus 26, 246–260 (2016). [PubMed: 26299904]
30. Berens P CircStat: A MATLAB toolbox for circular statistics. J. Stat. Softw 31, 1–21 (2009).

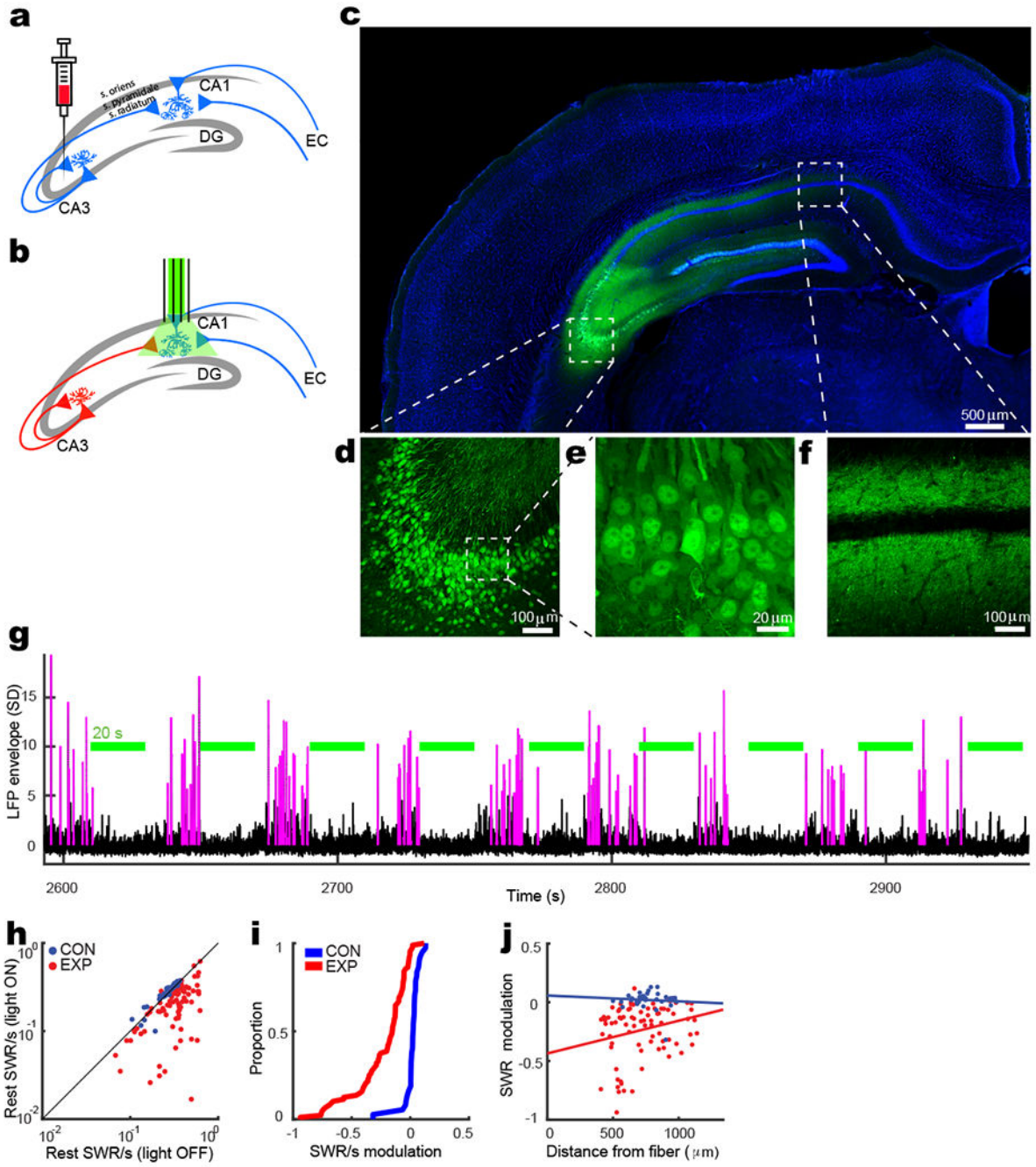

Figure 1: CA3 input is necessary for normal SWR activity in CA1.

a-b) Each rat undergoes two surgeries, the first for virus injection (**a**) and the second for bilateral "optetrode" implantation (**b**). **c-f)** An example of expression of virally-injected GFP in a coronal slice of rat brain (**c**). In a magnified view, CA3a pyramidal cells strongly express the GFP (**d** and **e**) and CA1 pyramidal cells receive CA3 inputs in their stratum radiatum and stratum oriens, above and below the cell layer, respectively (**f**). The blue background signal is from Hoechst 33258 staining. These results were independently repeatable for three more rats as shown in Supplementary Figure 1e. **g**) An example tetrode

in CA1 shows strong suppression of SWRs by silencing CA3 input to CA1. Magenta traces are periods in the LFP that meet SWR detection criteria. Green bars denote 20-s long light ON periods intermingled with 20-s light OFF periods. **h**) SWR incidence rate for each tetrode in light ON vs. light OFF conditions. Each dot represents a tetrode. CON: OFF: 0.26 ± 0.01 SWR/s (mean ± s.e.m.) and ON: 0.27 ± 0.01, two-tailed signed rank test, n = 37 tetrodes, $z_{(36)} = -3.3$, p = 0.0008; EXP: OFF: 0.34 ± 0.01 and ON: 0.22 ± 0.01, two-tailed signed rank test, n = 88 tetrodes, $z_{(87)} = 7.9$, $p = 5\times10^{-15}$. **i**) Cumulative density plot (CDF) of SWR incidence modulation index ([ON − OFF]/[ON + OFF]) (two-tailed rank-sum test: $n_1 = 37$ and $n_2 = 37$ tetrodes, $z_{(124)} = 7.8$, $p = 10^{-14}$). **j**) The relationship between the horizontal distance of each tetrode from optical fiber and the modulation of SWR incidence by light (Pearson's correlation, CON: r = −0.07, n = 37 tetrodes, two-tailed F-statistics, $F_{(36)} = 0.17$, p = 0.7; EXP: r = 0.18, n = 82 tetrodes, two-tailed F-statistics, $F_{(81)} = 4.59$, p = 0.02).

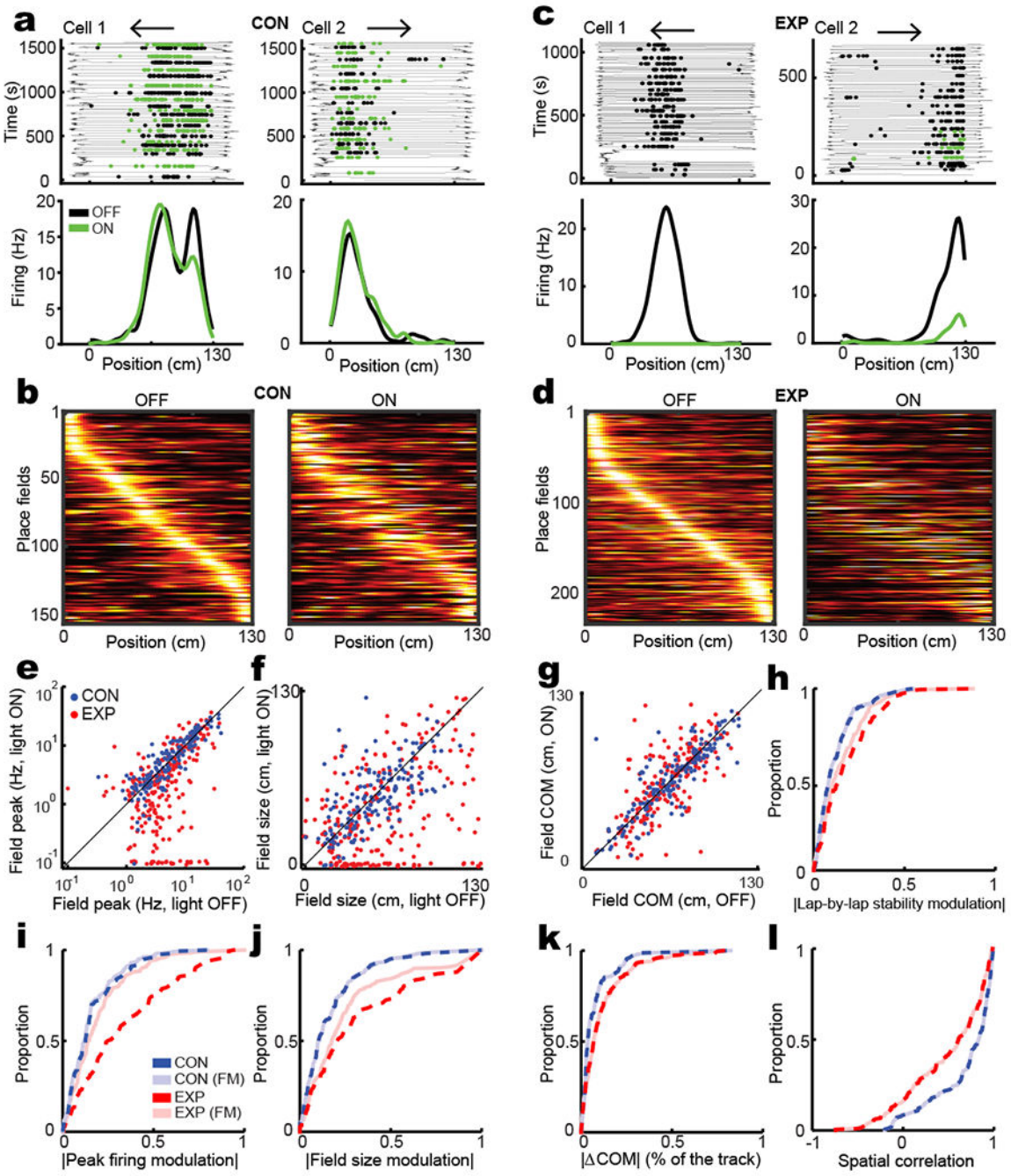

Figure 2: CA3 is necessary for normal place field responses in CA1.

a) Two example CA1 place fields in CON rats. Top: Rat position as a function of time during linear track traversals (thin line), overlaid with spiking activity only in the running direction depicted by the arrow. Spikes in light OFF and light ON conditions are shown as black and green dots, respectively. Bottom: The average place fields calculated from above lap-by-lap spiking activities. **b)** All non-repetitive CON place fields sorted by their peak firing position during light OFF condition on the linear track. Each row depicts the color map of same place field in light OFF (left) and light ON (right) conditions. Each field is

normalized by its maximum peak firing rate across OFF and ON conditions and the order of fields is similar between the two light conditions. **c-d)** Two example CA1 place field (c) and all non-repetitive sorted fields from EXP rats (**d**) as described in **a**-**b**. **e-g)** Place field features in light ON vs. light OFF conditions. Values are presented as mean ± s.e.m. **e)** Peak firing rate (CON: OFF: 7.97 ± 0.62 Hz and ON: 7.95 ± 0.55, two-tailed signed rank test, n = 157 fields, $z_{(156)} = -1.1$, p = 0.3; EXP: OFF: 6.63 ± 0.43 and ON: 4.70 ± 0.40, two-tailed signed rank test, n = 236 fields, $z_{(235)} = 5.8$, $p = 10^{-8}$). **f)** Place field size (CON: OFF: 51.40 ± 1.95 cm and ON: 51.01 ± 1.98, two-tailed paired t-test, n = 157 fields, $F_{(156)} = 0.06$, p = 0.80; EXP: OFF: 57.58 ± 2.17 and 39.97 ± 2.23; two-tailed signed rank test, n = 236 fields, $z_{(235)} = 6.8$, $p = 2\times10^{-11}$). **g)** COM (CON: OFF: 65.81 ± 2.02 cm and 65.81 ± 2.03, two-tailed paired t-test, n = 156 fields, $F_{(155)} = 0.00$, p = 1; EXP: OFF: 62.89 ± 1.54 and ON: 63.27 ± 1.81, two-tailed signed rank test, n = 207 fields, $z_{(206)} = -0.1$, p = 0.9). **h-l**) the CDF of place field features in CON and EXP rats. **h)** The CDF of the absolute value of the lap-by-lap stability modulation of original and firing-matched (FM) place fields (Original: two-tailed rank sum test, $n_1 = 156$ and $n_2 = 207$ fields, $z_{(362)} = -3.9$, $p = 2\times10^{-4}$; FM: two-tailed rank sum test, $n_1 = 156$ and $n_2 = 207$ fields, $z_{(362)} = -2.5$, p = 0.013; EXP original vs EXP FM: two-tailed signed rank test, n = 207 fields, $z_{(206)} = 4.2$, $p = 5\times10^{-5}$). **i)** The CDF of the absolute value of the amount of peak firing rate modulation (Original: two-tailed rank sum test, $n_1 = 156$ and $n_2 = 207$ fields, $z_{(362)} = -6.7$, $p = 3\times10^{-11}$; FM: two-tailed rank sum test, $n_1 = 156$ and $n_2 = 207$ fields, $z_{(362)} = -2.1$, p = 0.036). **j)** The CDF of the absolute value of the amount of field size modulation (Original: two-tailed rank sum test, $n_1 = 156$ and $n_2 = 207$ fields, $z_{(362)} = -5.1$, $p = 5\times10^{-7}$; FM: two-tailed rank sum test, $z_{(362)} = -3.4$, $p = 7\times10^{-4}$; EXP original vs EXP FM: two-tailed signed rank test, n = 207 fields, $z_{(206)} = 3.2$, $z_{(362)} = -3.0$, p = 0.0015). **k)** The CDF of the absolute value of the amount of COM shift (Original: two-tailed rank sum test, $n_1 = 156$ and $n_2 = 207$ fields, p = 0.0025; FM: two-tailed rank sum test, $n_1 = 156$ and $n_2 = 207$ fields, $z_{(362)} = -3.3$, p = 0.001; EXP original vs EXP FM: two-tailed signed rank test, n = 207 fields, p = 0.3). **l)** The CDF of the spatial correlation (Original: two-tailed rank-sum test, $n_1 = 156$ and $n_2 = 207$ fields, $z_{(362)} = 5.0$, $p = 10^{-6}$; EXP original vs EXP FM: two-tailed signed rank test, n = 207 fields, $z_{(206)} = 2.7$, p = 0.008).

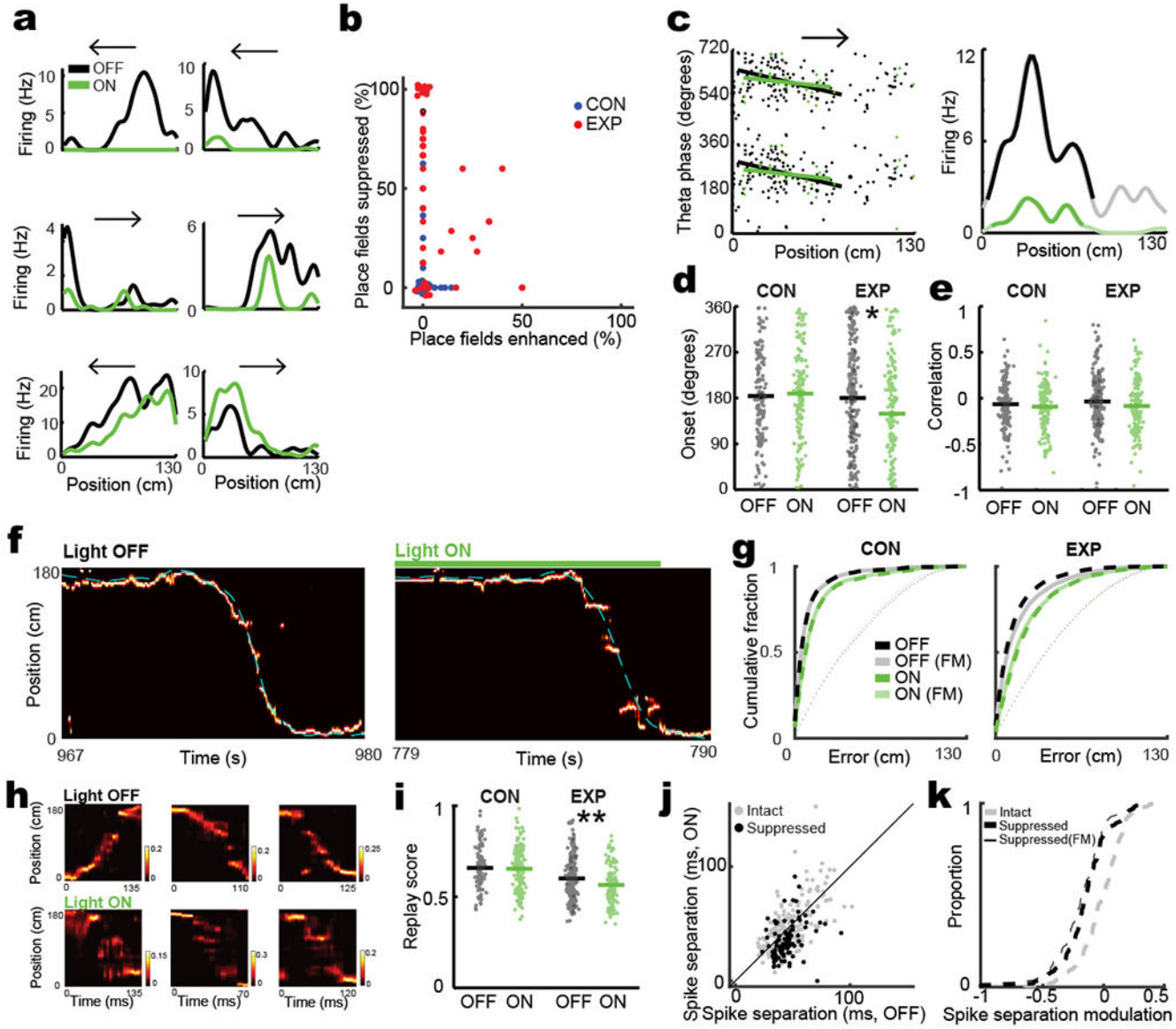

Figure 3: Effects of loss of CA3 input on theta precession in CA1 cells, and on CA1 ensemble activity

a) An example of six place fields simultaneously recorded from a single tetrode in an EXP rat. Arrow depicts running direction. **b)** Heterogeneity in place field responses of each tetrode (dot). For better visualization noise is added to the corners. Red dot with black circle represents the tetrode in (**a**). **c)** An example of phase precession in an EXP place cell. Left: each dot represents the theta phase of a spike occurring either during light OFF (black) or light ON (green) conditions in relation to rat's position on the track. Regression lines span the field range. Right: the corresponding place field in the two light conditions. Transparent color shows the overall firing and dark color shows the field range. **d-e)** Phase precession features presented in mean ± s.e.m. **d)** Precession onset (CON: OFF: 183.99 ± 6.02°, Rayleigh test for circular non-uniformity, n = 135 fields, $z_{(134)} = 8.8$, $p = 2\times10^{-4}$; ON: 188.72 ± 5.93, Rayleigh test, n = 144 fields, $z_{(143)} = 15.8$, $p = 5\times10^{-4}$; Watson-Williams test

for circular comparison, n_1 = 135 and n_2 = 144 fields, $F_{(278)}$ = 0.1, p = 0.7; EXP: OFF: 180.09 ± 5.18, Rayleigh test, n = 217 fields, $z_{(216)}$ = 2.8, p = 0.6 and ON: 149.34 ± 6.05°, Rayleigh test, n = 142 fields, $z_{(141)}$ = 6.2, p = 0.002; Watson-Williams test, n_1 = 217 and n_2 = 142 fields, $F_{(358)}$ = 5.0, p = 0.025). **e)** Precession correlation (CON: OFF: two-tailed t-test, n_1 = 135 and n_2 = 144 fields, $F_{(278)}$ = 0.7, p = 0.4; EXP: two-tailed rank-sum test, n_1 = 217 and n_2 = 142, $z_{(358)}$ = 1.7, p = 0.10). **f)** Bayesian decoding of rat's position as it traverses the linear track. Population posterior probability (heat plot) is overlaid with rat's actual position (cyan dashed line) in light OFF (left) and light ON (right, green bar) conditions. **g)** CDF of position reconstruction error (CON: two-tailed paired t-test, n = 4 sessions, $F_{(3)}$ = 3.4, p = 0.16; EXP: two-tailed paired t-test, n = 8 sessions, $F_{(7)}$ = 47.3, p = 0.0002; EXP FM: two-tailed paired t-test, n = 8 sessions, $F_{(7)}$ = 36.7, p = 0.0005; EXP OFF vs EXP OFF FM: two-tailed paired t-test, n = 8 sessions, $F_{(7)}$ = 7.6, p = 0.028). Dotted lines show the chance level of reconstruction error in two light conditions. **h)** Examples of replays occurring during light OFF (top) and light ON (bottom) conditions in EXP rats. Each panel shows posterior probability of a decoded replay with its corresponding scale bar. **i)** Replay score (CON: two-tailed t-test, n_1 = 99 and n_2 = 148 replays, $F_{(245)}$ = 0.1, p = 0.8; EXP: two-tailed rank-sum test, n_1 = 212 and n_2 = 121 replays, $z_{(342)}$ = 2.6, p = 0.0098). bars represent mean ± s.e.m. **j)** In-SWR spike separation in "intact" and "suppressed" pairs (Intact: OFF: 47.75 ± 1.18 (mean ± s.e.m) ms and ON: 48.34 ± 1.75, two-tailed signed rank test, n = 194 field pairs, $z_{(193)}$ = 0.2, p = 0.8; Suppressed: OFF: 45.09 ± 1.10 and ON: 35.60 ± 1.52, two-tailed signed rank test, n = 102 field pairs, $z_{(101)}$ = 5.7, p = 2×10^{-8}). **k)** The CDF of spike separation modulation (Intact vs. Suppressed: two-tailed t-test, n_1 = 194 and n_2 = 102 field pairs, $F_{(294)}$ = 29.9, p = 10^{-7}; Suppressed vs. Suppressed FM: two-tailed t-test, n_1 = 102 and n_2 = 82, $F_{(182)}$ = 1.8, p = 0.19). *P< 0.05, **P< 0.01, ***P< 0.001.